A FAST 3D NON-ITERATIVE APPROACH TO PRESSURE CALCULATION FROM PC-MRI: PHANTOM EXPERIMENTS

MJ Negahdar[1], Mo Kadbi[1], JungWon Cha[1], Juan Cebral[2], and Amir Amini[1]

[1]*Electrical and Computer Engineering, University of Louisville, Louisville, Ky, United States,* [2]*School of Computational Sciences, George Mason University, Fairfax, VA, United States*

Introduction: Phase contrast MRI is widely used to noninvasively measure blood velocity and flow in vivo[1]. PC-MRI can derive all three velocity components within a 3D imaged volume. The velocity field can then be used to obtain flow pattern, wall shear stress, vascular compliance, blood pressure, and other hemodynamic information. The relative pressure drop across a stenotic narrowing provides an important indication regarding the hemodynamic severity of a stenosis and is a significant physiologic parameter in the planning of revascularizations.

The law of conservation of momentum (Navier-Stokes equation), governs motion of Newtonian fluids. If we assume that viscosity is constant, Navier-Stokes equation can be written as: $\widehat{\nabla P} = -\rho\frac{\partial u}{\partial t} - \rho(u.\nabla)u + \mu\nabla^2 u + \rho f$ where u(x,y,z,t) is the fluid vector velocity from PC MRI, P is the scalar pressure, ρ is the density of the fluid and f is the body force. Due to the noise in PC-MRI velocity data, the pressure gradient field $\widehat{\nabla P} = (\widehat{P_x}, \widehat{P_y}, \widehat{P_z})$ is not curl-free, and therefore it cannot be the true gradient of the scalar pressure field. An extremum principle is cast to find P such that ∇P is the projection of $\widehat{\nabla P}$ onto the curl-free subspace of integrable vector fields. The conventional approach to the corresponding numerical optimization is based on the iterative solution to the pressure-Poisson equation[2].

Non-Iterative Harmonic-Based Orthogonal Projection: In lieu of the iterative approach, and provided a series of orthogonal integrable basis function $\phi(x, y, z, \varpi)$ with ϖ as the vector $(\omega_x, \omega_y, \omega_z)$ of spatial frequencies, the pressure $\widetilde{P}$ can be expanded as: $\widetilde{P} = \sum \widetilde{C}(\varpi)\, \phi(x, y, z, \omega)$. Its gradients will have $\widetilde{P_l} = \sum \widetilde{C}(\varpi)\, \phi_l(x, y, z, \omega)$, with $\phi_l = \frac{\partial\phi}{\partial l}$ and $l = x, y, z$. The measured gradient can also be expanded as $\widehat{P_l} = \sum \widehat{C_l}(\varpi)\, \phi_l(x, y, z, \omega)$. Following Frankot and chellappa[3], the coefficient of expansion of the projected pressure $\widetilde{P}$ onto an integrable subspace, is related to $\widehat{C_x}, \widehat{C_y}$, and $\widehat{C_z}$ by $\widetilde{C} = \frac{\widehat{C_x}\,T_x + \widehat{C_y}\,T_y + \widehat{C_z}\,T_z}{T_x + T_y + T_z}$ where $T_l = \int_{\mathbb{R}^3} |\phi_l|^2\ dx\,dy\,dz$. Therefore, by substituting $\widetilde{C}(\varpi)$ into equation for $\widetilde{P}$, integrable pressure gradients and the correctly integrated pressure field can be obtained. Note that the pressure field is reconstructed in one-pass (with no iterations) using all of the available information in $\widehat{P}_x$, $\widehat{P}_y$ and $\widehat{P}_z$.

In this paper, Fourier basis functions are adopted for $\phi(\varpi)$ for convenience and speed of computation offered using the fast Fourier Transform (FFT). The key differences between Frankot and Chellapa's[3] method and our method are: (i) Since FFT needs to be applied to a 3D cubical domain, while PC velocity information is only available within the vessel lumen, the PC data needs to be extrapolated at the boundaries in order to remove discontinuities and (ii) FFT assumes that the data is periodic and, therefore, a discontinuity in the periodic extension of pressures will exist which once again needs to be removed.

Imaging: Experiments were carried out using a closed loop flow system with an 87% area stenotic narrowing under constant flow Q=13.2 ml/s (Reynolds number = 160) and Q=39.6 ml/s (Reynolds number = 480). Imaging was performed on a Philips Achieva 1.5T scanner (Philips Healthcare, Best, NL) using an 8 element phased-array knee RF coil. To measure the velocities, a multi-slice 2D turbo gradient echo sequence was utilized that included a bipolar velocity encoding gradient in a single predetermined direction. Conventional Cartesian trajectory was chosen for image acquisition. The remaining sequence parameters were as follows: FOV = 96x96 mm, 1.5x1.5 mm acquired in-plane resolution, 4 mm slice thickness, flip angle = 5, matrix size = 64x64, TR/TE = 7.6/4.4 ms (Re = 480) and 8.0/5.0 ms (Re = 160).

CFD: Computational Fluid Dynamic (CFD) simulations were carried out for two steady flow experiments by solving the 3D unsteady Navier-Stokes equations were numerically solved using the finite element formulation. For this purpose, the geometrical model of stenotic phantom was reconstructed from high-resolution CT and a finite element grid covering the conduit was generated. The computational grid contained about 8 million tetrahedral elements.

Results: Two types of comparisons were made: in one instance, the pressures derived from noise-corrupted CFD velocities using both the new 3D non-iterative pressure calculation technique as well as the iterative solution to pressure-poisson equation were compared with CFD simulated pressures. In a second instance, the pressures derived from in-vitro MRI studies were compared with pressures directly generated with CFD. In adding noise to CFD-simulated velocities, Gaussian distributed noise with zero mean and variance of σ^2 was used. Table 1 reports the relative error $R.E. = \frac{PD_c - PD_{CFD}}{PD_{CFD}} * 100\ \%$ in computing the pressure drop (PD) between the calculated pressures and CFD simulated pressures for a range of standard deviation for noise. As can be seen in table1, the non-iterative method is a bit more sensitive to noise rather than iterative method, however results are still in acceptable range.

Figure 1 shows comparison between 3D CFD simulated pressures and 3D calculated pressures by iterative and non-iterative techniques for Reynolds numbers of 160 and 480 for in-vitro MRI data. As may be seen, the iterative method slightly underestimates the pressures relative to the non-iterative method. Finally, for the in-vitro studies described here, the computational time for obtaining the relative pressures was 4.83 seconds on a quad core 2.4 GHz CPU processor with 8GB of memory for deriving the 3D pressure field from 50 axial PC MRI slices. This is to be compared with 87.4 seconds for the iterative approach on the same platform.

	σ	0.00	0.02	0.04	0.06	0.08
Flow Regime	**Method**	**R.E.**				
Re=160	Iterative	8 %	7 %	6 %	8 %	2 %
	Non-iterative	12 %	11 %	7 %	0 %	3 %
Re=480	Iterative	7 %	7 %	9 %	8 %	4 %
	Non-iterative	14 %	13 %	10 %	5 %	2 %

Table 1. Relative error (R.E.) when comparing the pressure drop between the calculated and CFD simulated pressures for both iterative and non-iterative methods for Reynolds number 160 and 480 for a range of additive Gassuian noise powers.

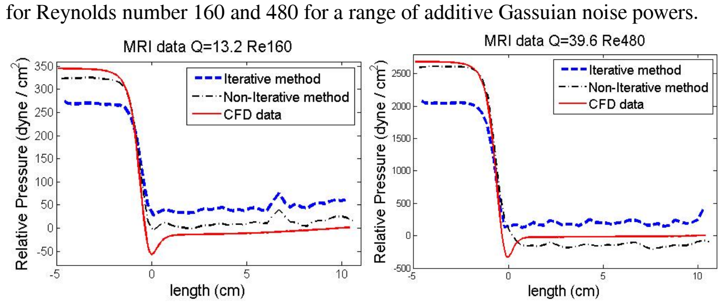

Figure 1: Comparison of CFD simulated pressures (red line) with those calculated with the iterative method (blue dotted line) and non-iterative method (black dotted line) using in-vitro PC-MRI data for constant flows with Reynolds numbers Re = 160 (left) and Re = 480 (right). Please note that only pressure along the centerline of the phantom has been displayed.

Discussion and Conclusion: In this paper, we have introduced a new 3D non-iterative method which results in significant computational savings for calculation of intravascular pressures from phase-contrast MRI while providing good accuracy. Results from simulations and in-vitro phantom studies showed good agreement between the new non-iterative method and the conventional iterative method and pressure maps directly generated by CFD. As demonstrated, when using Fourier basis functions, the algorithm applies three 3D FFT's and one inverse 3D FFT to arrive at the results.

Future work will involve application of the method to pulsatile stenotic flows in phantom experiments as well as to data acquired in patients with atherosclerotic disease.

References: [1] N. J. Pelc, et al., *Magn Reson Q,* vol. 10, pp. 125-47, Sep 1994. [2] G.-Z. Yang, et al., Magnetic Resonance in Medicine, vol. 36, pp. 520-526, 1996. [3] R. T. Frankot, et al., IEEE Transactions on Pattern Analysis and Machine Intelligence, vol. 10, pp. 439-451, 1988.